ARTICLE NO. 79-0462R

C 80-070

Drag and Pressure Distribution on a Family of Porous, Slotted Disks

00001
00008

Bryan W. Roberts*
University of Sydney, Sydney, Australia

To investigate the effect of porosity in ribbon parachutes, the flow over a series of flat, circular disks has been studied in detail. These disks have been fabricated with 1-18 concentric slots covering a geometric porosity range from 2% to 33% open-area ratio. On one disk the rear edges of each slot have been chamfered at 45 deg to fix the separation points at all test Reynolds numbers. All outside diameters were chamfered. The disk drag and pressure distributions have been measured, and the results compared to those for a solid disk. Base pressure coefficients behind the solid, or ribbon, elements show surprisingly low values.

I. Flow Through an Infinite Rigid Screen

A. Introduction

MANY studies have been made of the flow through and about porous screens. The majority of the studies have examined the flow through porous plates and sheets of infinite extent. It is important to appreciate from the outset that numerous studies have examined the flow through porous bodies of infinite extent, while only a few studies have examined the simultaneous flow through and around porous bodies for finite extent. The latter work is much more difficult than the former; it is the latter problem which is of interest to workers in the parachute area.

The flow through infinite, porous, rigid membranes such as grids, plates, or sheets are usually made by locating the element in a parallel tube, pipe, or channel. The flow approaching the element is known, and the pressure drop coefficient or resistance coefficient k is measured as a function of the Reynolds number, usually characterized by a pore or element size. The porosity λ of the membrane is also significant.

Structural distortion of the porous membrane often occurs due to the aerodynamic loading. This effect contributes greatly to the complexity of the problem, and this phenomenon is important in the parachute context.

In the parachute situation the relevant issue is not what the value of the resistant coefficient is, but what is the value of the drag coefficient C_D of the complete aerodynamic body when it is placed in an infinite flowfield? Of course, the latter question should involve a determination of the local resistant coefficient when the system is under stress.

In this sort of study, the flow approaching the porous parachute or porous disk produces a drag which is generally a function of the porosity and possibly two Reynolds numbers. One of these Reynolds numbers is based on the body's characteristic length, while the other relates to a characteristic pore size. Relatively few studies have been made of this class of problem, but a few typical references are Refs. 6-10.

In view of the preceding remarks, it has been decided to present this paper in two parts. The first briefly reviews the form of the resistance coefficient for porous, rigid screens of infinite extent. The second part examines the flow through and around a porous, rigid body of finite extent. This body will be located in an infinite flowfield, and will be rigid and incapable of significant distortion under the aerodynamic loading. Experimental results for tests on porous, circular disks will be given in Part II.

Furthermore, it will be argued and demonstrated in Part II that a macroscopic examination of the flowfield neglects an important phenomenon which relates to the microscopic flow structure behind the adjacent small elements within the porous body. References 6-8 and 10 all relate to various macroscopic treatments.

B. Flow Through an Infinite, Porous, Rigid Screen

As mentioned in the Introduction it is worthwhile to briefly consider the normal flow through an infinitely large porous, rigid screen or sheet. The screen is assumed to be rigid in that the aerodynamic loading produces deformations which are small relative to the pore size of the screen. This rigidity may be practically realized by using metal screens or suitably perforated metal plates.

The resistance coefficient k for a two-dimensional screen system can be defined according to Taylor and Davies[1] or Hoerner[8] as

$$k = (p_1 - p_2) / \tfrac{1}{2}\rho V_0^2 \tag{1}$$

where V_0 is the velocity of the fluid a long way upstream and p_1 and p_2 are the static pressures a long way upstream and downstream.

The geometric porosity, or open-area ratio, of the screen can be denoted by λ, while Hoerner uses the solidity ratio σ in lieu of λ. There is, however, the simple relationship

$$\sigma = (1 - \lambda) \tag{2}$$

Now the relationship between k and λ depends critically upon whether the screen is composed of sharp-edged elements or more streamlined elements. In the former case, the value of k is not highly dependent upon the value of the pore Reynolds number because the separation points are fixed at the edges of the sharp elements.[1] However, in the latter case, the value of k is dependent on the pore Reynolds number, particularly when this Reynolds number is less than 1000. This latter effect is to be expected as the location of the separation points within the elements of the screen are highly Reynolds number dependent at this Reynolds number scale.

Each of these two cases involving sharp and streamlined screen elements will now be examined in detail. These two

Presented as Paper 79-0462 at the 6th Aerodynamic Decelerator & Balloon Technology Conference, Houston, Texas, March 5-7, 1979; submitted May 2, 1979; revision received Nov. 9, 1979.

Index categories: Deceleration Systems; Aerodynamics.

*Associate Professor, Dept. of Mechanical Engineering. Member AIAA.

cases are important in connection with parachutes. For ribbon parachutes, the ribbon elements are sharp-edged, while fabric parachutes may be taken as being circular elements approximating to the threadlike components.

1. Resistance Coefficient of a Screen with Sharp-Edged Elements

Taylor and Davies[1] have postulated that the resistance coefficient can be expressed as

$$k=\left(\frac{1-\gamma}{\lambda^2 C^2}\right)-1 \tag{3}$$

where C is the vena-contracta coefficient associated with the local flow through the sharp-edged pores. On the other hand, γ is the pressure recovery coefficient that quantifies the magnitude of the static pressure recovered by the stream after it passes through the vena-contracta region. Taylor and Davies[1] have used O'Brien and Hickson's values for $C(\lambda)$ to produce the dotted curve shown in Fig. 1. The dotted curve assumes $\gamma=0$ and that C is asymptotic to 0.61 as $\lambda\to 0$ after Milne-Thompson.[11]

The next step is to assume a typical value for γ. Taylor and Davies[1] suggest that γ is approximately 0.4. The present author[12] has determined the parameter experimentally to be 0.42 when the solid element Reynolds number is of the order of 10^4.

Therefore, it follows from Eq. (3) that

$$k=0.58/\lambda^2 C^2-1 \tag{4}$$

Equation (4) is shown in Fig. 1 as the solid curve. This curve is in excellent agreement with Taylor and Davies' and Simmons' experiments shown in Fig. 1. It is important to note that all the experimental points have been determined using rigid screens and that the separation points within the pores are most likely located at the sharp edges within the screen. As such, one would expect the value of k to be independent of Reynolds number, when this number is based on the pore or solid element size (see Ref. 1, p. 395). Furthermore, the solid curve in Fig. 1 compares favorably with the published work of Hoerner (see Ref. 8, Fig. 43).

Finally, it is worth pointing out that in the subsonic or transonic ribbon or ring slot parachute situation, typical values for λ and pore Reynolds number N_p are

$$0.05\le\lambda\le 0.35$$

$$10^4\le N_p\le 10^6$$

Work due to Betz and Petersohn[18] and Birkhoff et al.[19] has been cited by Gurevich.[17] Both groups of workers have considered a free streamline flow about a two-dimensional screen made up of flat plate elements. This screen flow is equivalent to the flow past a single flat plate which is mounted centrally in a channel of finite width. The results of the theoretical determination of k by these workers make an interesting comparison to that given by Taylor and Davies.[1] A comparison is made in Fig. 2 where the results of Taylor have been taken from Fig. 1. This is shown as the right-hand curve in Fig. 2. The work of Betz et al. and Birkhoff et al. is shown as the left-hand set of curves in Fig. 2.

The upper three, near-coincident curves in Fig. 2 have been derived on solely theoretical grounds. Taylor's theory uses a vena-contracta approach, while Betz and Birkhoff use a free streamline theory. The experiments due to Betz are shown as circles on the figure, while Taylor's works are given by squares. In all cases, Betz's values are higher than Taylor's. This is because Betz measured his pressure just behind the screen, while Taylor measured his some fifty grid element lengths downstream. Thus, Taylor's points have a significant pressure recovery effect while Betz's points have none. This discrepancy is not a Reynolds number effect, but simply a lack of similarity in the definition of the downstream pressure location.

2. Resistance Coefficient of a Screen with Circular Section Elements

If the infinite, rigid porous screen is composed of circular elements, as in a wire gauze, then the situation is no longer described by Eq. (4).

Screens or gauzes made from circular elements are highly Reynolds number dependent. It is suggested that if the Reynolds number based on the elemental diameter is less than about 8×10^4, when λ is of the order of 0.3, then the boundary layer on the grid elements is laminar. At much higher Reynolds number, the boundary layer may suffer a turbulent separation. Taylor and Davies[1] also note (p. 397) that the resistance coefficient is highly Reynolds number dependent.

However, if the circular element Reynolds number is of the order of 10^3, we will postulate that the vena-contracta effect is absent,[13] and that the pressure recovery coefficient is unchanged at 0.42. Therefore, Eq. (4) can be extended to the present case when C tends to unity and hence

$$k=0.58/\lambda^2-1 \tag{5}$$

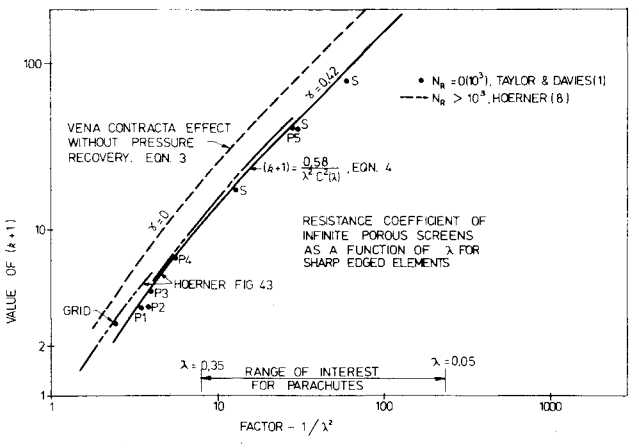

Fig. 1 Sharp edged resistance coefficient.

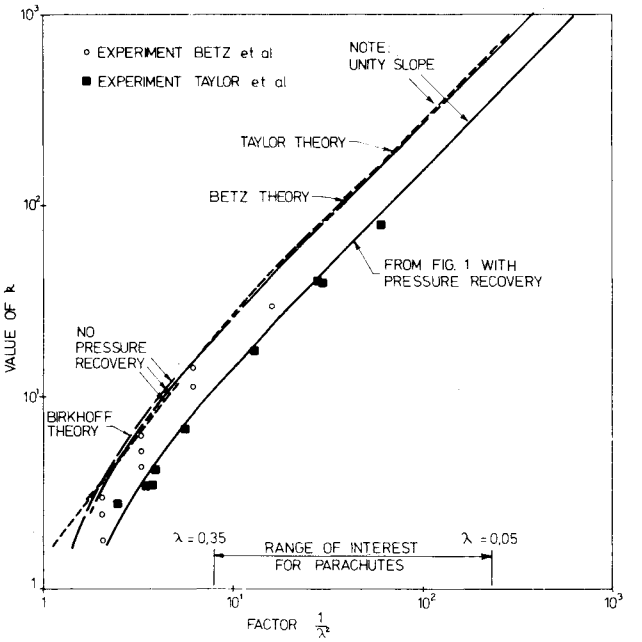

Fig. 2 Comparison of theories by Taylor and Davies,[1] Betz and Petersohn,[18] and Brikhoff, Plesset, and Simmons.[19]

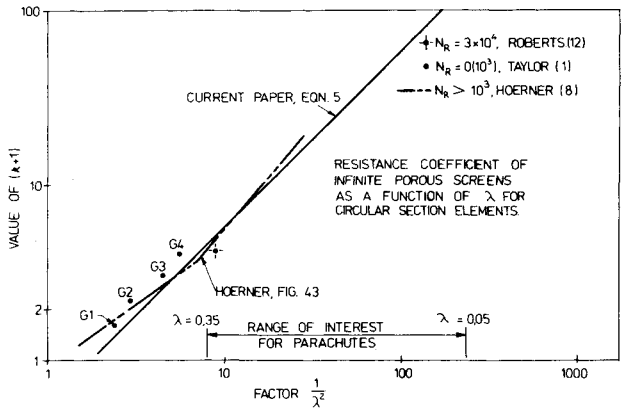

Fig. 3 Circular section resistance coefficient.

Equation (5) has been drawn in Fig. 3 for comparison with the results of Ref. 1. In addition, Hoerner's results[8] are also plotted for comparison purposes.

It can be seen in Fig. 3 that Eq. (5) somewhat underpredicts Taylor's results by about 20%. On the other hand, the current postulate is in excellent agreement with Hoerner's curves when the Reynolds number is in excess of 10^3.

If we were to consider a screen of parachute-type fabric whose porosity λ was measured at the relevant aerodynamic loading, then typical values would be

$$0.05<\lambda<0.35$$

$$10<N_s<10^3$$

where N_s is the Reynolds number based on the circular element diameter.

C. Drag Coefficient of a Porous, Circular Disk

In Sec. II we briefly summarized the form of the resistance coefficient for various types of infinite, rigid porous screens. More details abound in the literature; yet, only relatively few observations have been made of the drag coefficients of finite-sized, porous aerodynamic bodies. More information on porous bodies is applicable to parachutes of various sizes and shapes.

The parachute, however, is a rather difficult system on which to study the effects of porosity on the drag coefficient. For example, the conventional parachute is a deformable structure whose flying shape is too imprecise for accurate drag measurement. Furthermore, the value of k is too imprecise since the parachute fabric or ribbons are deformed and disorientated under any imposed aerodynamic loading.

In short, the parachute will not be examined at this time. Instead, we will endeavour for the moment to examine the flow about a more precise aerodynamic, porous structure; namely, the porous disk.

The flat, rigid disk has been chosen for detailed examination. The main advantage of the disk is that it may be accurately constructed and mounted, while the disk structure can be made of sufficient thickness in order to eliminate distortion under aerodynamic loading.

II. Flow Through and Around Finite-Sized Porous Disks

A. Various Methods of Analysis for the Flow about Porous Disks or Plates

A number of theoretical techniques will now be examined. These techniques all relate to the analysis of the flow through and around porous screens of various shapes placed normal to the flow. Three of the available methods are given in the following.

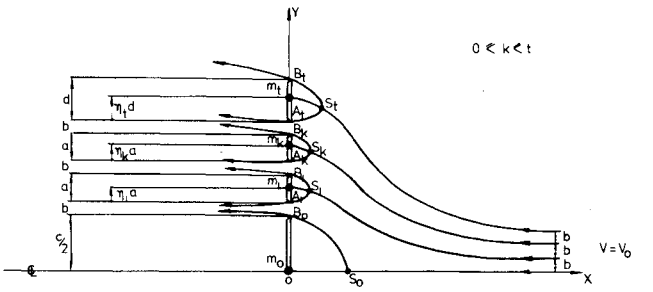

Fig. 4 Source flow model for the flow about a finite screen.

1. Source Distributions in Two-Dimensional Flowfields

It is well known that forces in potential flow may arise due to sources located in the flowfield. Such models are the bases for most theoretical studies on two-dimensional or axisymmetric porous screens.

Taylor and Davies[1] considered a uniform, two-dimensional source distribution of strength $\frac{1}{2}ku$, where u is the velocity through the screen. In this manner, the authors were able to calculate that the drag coefficient of a two-dimensional screen was

$$C_D = k/[1+\tfrac{1}{4}k]^2 \tag{6}$$

Koo and James[16] have extended the basic Taylor model to arbitrary shaped screens of finite widths. In all cases the screens were placed in channel flows and were imagined to be a continuous distribution of sources. By choosing two matching conditions at the screen, it was possible to calculate the source distribution and the so-called attenuation function. For a two-dimensional, uniform, normal screen in an infinite flowfield, they found that the drag coefficient is given by the relationship

$$C_D = k/[1+\tfrac{1}{2}Dk]^2 \tag{7}$$

where $D(\lambda)$ is given in Fig. 3 of Ref. 16.

A somewhat different approach has been taken by the present author. It is argued that a solid element in a two-dimensional screen may be represented by a two-dimensional line source. The magnitude and location of each source is carefully chosen so that the stagnation streamlines always pass through the sharp edges of each element within the porous screen. This flow condition may be seen in Fig. 4. Therein, a two-dimensional screen is equally located on either side of the OX axis.

On the kth element a source of strength m_k is located at a point $\eta_k a$ from the lower edge A_k of the kth element. The upper edge of this element is labeled as B_k. This kth source is now located in the infinitely thin normal screen so that the kth stagnation streamline through the point S_k divides and passes precisely through the points A_k and B_k. Remembering from the preceding that A_k and B_k are the extreme edges of the kth sharp-edged element in the screen under discussion, it should be noted that the central screen element width is c, the outermost element width is d, all remaining elements widths are a, and the width of each opening is b. The total number of slots or openings in the two-dimensional array is t.

Expressions for the stream function at points A_0, A_k, B_k, A_t, and B_t immediately follow as

$$\psi_{B_0} = \psi_{S_0} = (\pi m_0/2) - (V_0 c/2) \tag{8}$$

$$\psi_{A_k} = \psi_{S_k} = \frac{\pi m_0}{2} + \pi \sum_{n=1}^{k} m_{n-1} - V_0\left\{(k-1)a + \frac{c}{2} + kb\right\}$$

$$\text{for } k = 1,2,\ldots,t \tag{9}$$

$$\psi_{B_k} = \psi_{S_k} = \frac{\pi m_0}{2} + \pi \sum_{n=1}^{k} m_n - V_0 \left\{ ka + \frac{c}{2} + kb \right\}$$

$$\text{for } k = 1,2,\ldots,(t-1) \tag{10}$$

$$\psi_{B_t} = \psi_{S_t} = \frac{\pi m_0}{2} + \pi \sum_{n=1}^{t} m_n - V_0 \left\{ (t-1)a + \frac{c}{2} + d + kb \right\} \tag{11}$$

From the preceding equations, it follows that

$$m_0 = V_0 c/\pi \tag{12}$$

$$m_k = V_0 a/\pi \qquad k = 1,2,\ldots,(t-1) \tag{13}$$

$$m_t = V_0 d/\pi \tag{14}$$

and

$$\psi_{S_k} = V_0 kb \tag{15}$$

Because all of the sources are located on the Y axis in Fig. 4, the u velocity at any station along this axis is equal to V_0. As a consequence of this fact, it follows that the stagnation streamlines for upstream and downstream are spaced a distance b apart.

Next, by Lagally's theorem the total force, F_k, on any source m_k is proportional to that source strength times the velocity at that point V_k with the kth source removed. Thus we have

$$F_k = 2\pi\rho m_k V_k \tag{16}$$

But we know that

$$V_k = V_0 i + v_k j \tag{17}$$

where V_k is the perturbation velocity at the kth source and

$$F_k = X_k i + Y_k j \tag{18}$$

Finally, we can combine Eqs. (12-18) to show that

$$\begin{aligned} X_0 &= 2\rho V_0^2 c \\ X_k &= 2\rho V_0^2 a \\ X_t &= 2\rho V_0^2 d \\ Y_0 &= Y_k = Y_t = 0 \end{aligned} \tag{19}$$

The simple result, by addition of all the terms in Eq. (19), is that the total screen drag is proportional to the total closed area of the gauze. That is,

$$X = 2\rho V_0^2 [c + 2d + a(t-1)] \tag{20}$$

Furthermore, it can be easily shown that the porosity λ of the screen under consideration is given by

$$\lambda = 1 - \left[\frac{c + 2d + a(t-1)}{c + 2d + a(t-1) + tb} \right] \tag{21}$$

Now if C_D^* is defined as the drag coefficient of an impervious, two-dimensional screen, then the drag coefficient C_D of our porous screen is simply given by

$$C_D = C_D^* (1 - \lambda) \tag{22}$$

and

$$C_D^* = 4 \tag{23}$$

This value for C_D^* is primarily determined by the boundary condition of the stream function at points S_k, A_k, and B_k. This numerical value for C_D^* is approximately double the experimental value, which is 1.98 for a flat plate.

However, it is important to note that the theoretical drag coefficient of a porous disk reduces proportionally to the reduction in the solidity ratio for a finite width, two-dimensional screen.

2. Free Streamline Theories in Two-Dimensional Fields

Another interesting approach to the whole question is the European and Russian work. There are a number of examples where the flow about a two-dimensional sharp-edged screen has been analyzed by a free streamline technique. In this method, free streamlines are assumed to originate from each of the elements within the porous screen. One of the simplest and yet most intriguing solutions to the porous plate problem may be found page 182 of Ref. 17. Therein Bonder is reported to have examined the separated flow about two adjacent, identical plates placed normal to the flow. The physical situation is shown in Fig. 5. It was found that this single slotted plate in Kirchoff flow (wake underpressure coefficient $\sigma = 0$) had a total drag coefficient based on the solid area, which was independent of the spacing b between the plates. It was found that

$$C_D = \frac{D}{\frac{1}{2}\rho V_0^2 \cdot 2a} = 2\pi/(4+\pi) \tag{24}$$

Equation (24) can be expressed in terms of the porosity of the assembly to show that

$$C_D = 2\pi/(4+\pi)(1-\lambda) \tag{25}$$

where

$$\lambda = b/(2a+b) \tag{26}$$

It is useful to note the similarity between Eqs. (22) and (25). They are identical except for the numerical value of C_D^*.

Finally, there is, by all accounts, a powerful, free streamline theory for finding the flow about n curvilinear plates or arcs. This so-called Sedov method[20] (pp. 194-199) is also referred to by Gurevich[17] (pp.119-123). Ambrovii[21] has also solved the problem of n parallel flat plates, but his work is presently unobtainable in the western literature.

3. Approximate Macroscopic Theory

The current author along with Nhan[14] has produced another theory which is essentially as shown in Fig. 6. A porous disk of radius R_0 is situated in a freestream of velocity V_0. The disk is assumed to be composed of a large number of small pores through which the fluid may pass.

A small surface element ds will contain a cluster of pores through which the fluid flows at a velocity v_n based on the total elemental area. This pore flow is induced by a pressure

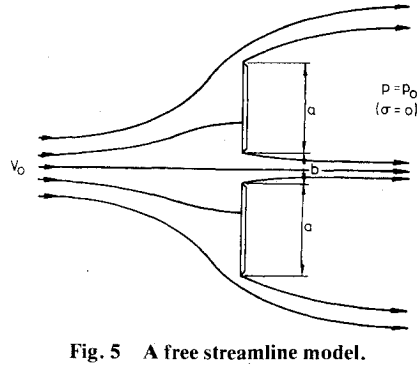

Fig. 5 A free streamline model.

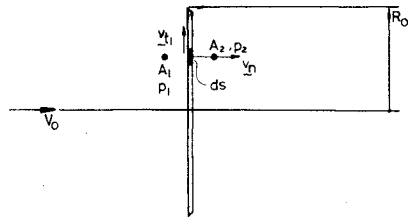

Fig. 6 A macroscopic theory.

differential $(p_1 - p_2)$ at points A_1 and A_2, respectively. Superimposed on the preceding normal flow is a local tangential flow v_{t_1}.

Next, we will assume that the porosity at the surface is in the parachute range, namely

$$0.05 < \lambda < 0.35$$

so that the local resistance coefficient is in the range

$$0(5) < k < 0(200)$$

If k lies in this range, it is reasonable to assume, according to Ref. 15, that the tangential velocity is unchanged by the crossflow v_n at the disk surface.

If we begin with the definition of k as

$$k = (p_1 - p_2) / \tfrac{1}{2}\rho V_0^2 \tag{27}$$

then this equation may be rewritten

$$(v_n / V_0)^2 = (p_1 - p_2) / \tfrac{1}{2} k \rho V_0^2 \tag{28}$$

Next, introduce pressure coefficients C_p normalized on the dynamic pressure to show that

$$(v_n / V_0)^2 = (C_{p_1} - C_{p_2}) / k \tag{29}$$

From the definition of the pressure coefficient, it follows that

$$C_{p_1} = 1 - (v_1 / V_0)^2 = 1 - (v_{t_1} / V_0)^2 - (v_n / V_0)^2 \tag{30}$$

and on substitution of Eq. (29) in Eq. (30) one obtains

$$C_{p_1} = 1 - (v_{t_1} / V_0)^2 - (C_{p_1} - C_{p_2}) / k \tag{31}$$

If the pressure coefficient at point A_1 is $C^*_{p_1}$, when the plate is impervious, then by Thwaites's assumption, $C^*_{p_1}$ may be written as

$$C^*_{p_1} = 1 - (v_{t_1} / V_0)^2 \tag{32}$$

Next, substitute Eq. (32) into Eq. (31) to give

$$C_{p_1}(k+1) - C_{p_2} = k C^*_{p_1} \tag{33}$$

Likewise, if the pressure in the wake is assumed to be unchanged by a small base bleed of v_n, then the base pressure averaged over the solid elements of the porous disk gives

$$C_{p_2} = (1 - \lambda) C^*_{p_2} \tag{34}$$

Hence, Eqs. (33) and (34) give Eq. (35) when the pressure differential is integrated over the disk.

$$C_D = \left(\frac{k}{k+1}\right)\left[C^*_{p_1} + \frac{\lambda}{\pi R_0^2}\int_{\text{rear}} C^*_{p_2}\, ds\right]$$

$$= \left(\frac{k}{k+1}\right)\left[C^*_D - 0.45\lambda\right] \tag{35}$$

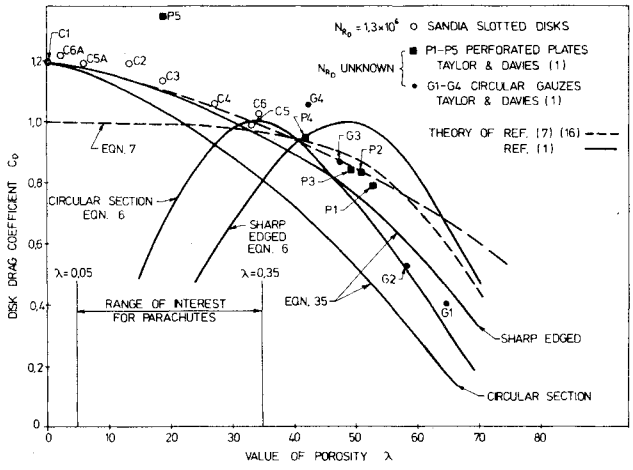

Fig. 7 Drag coefficients.

The integral in Eq. (35) has been evaluated knowing that $C^*_{p_2} = -0.45$ for solid disks.

B. Some Experimental Drag Coefficients for Porous Disks

The published data of Taylor and Davies,[1] along with some current experiments, have been compared with Eq. (28) in Fig. 7. In this figure it can be seen that the measured drag coefficients are apparently in good agreement with Eq. (35). The two-dimensional theory of Koo and James[16] is also shown, along with the classical Taylor and Davies[1] two-dimensional formulae of $C_D = k/(1 + k/4)^2$. The latter theory is unsatisfactory for porosities less than 50%, or when $k > 4$, as previously noted by Graham.[7]

At low values of porosity, which are applicable to the parachute range of interest, one might come to the following conclusions. It would appear at first sight that the results of Fig. 7 are adequately described by Eq. (35). However, in Figs. 7 and 2 of Graham's work,[7] there exists considerable scatter which cannot be attributed to the measurement of the drag force or dynamic pressure. For example, the current experiments on the so-called "Sandia Slotted Disks" are accurate to better than 1%, while the apparent scatter is 5% or more.

This scatter effect can be examined further by reference to Fig. 8. This figure shows the drag coefficient of eight slotted disk configurations all measured at comparable Reynolds numbers. The geometric details of the disks are shown in Table 1.

Figure 8 shows that the porosity λ does not uniquely determine the drag coefficient of a porous disk. Figure 8 is applicable to a Reynolds number of 1.3×10^6 based on the disk diameter. Similar trends were observed at all Reynolds numbers in the range 9.1×10^4 to 1.6×10^6.

In fact, it can be seen that the drag coefficient of the disks may actually be increased over and above the solid disk drag by the introduction of a nominal amount of porosity. It can also be inferred from Fig. 8 that the drag may be increased by increasing the number of slots N while the porosity and Reynolds number are held constant. The latter statement is confirmed by comparing configurations 5 and 6.

This apparent imprecision in the drag coefficient will now be investigated in detail by examining the actual pressure distributions on this family of disks.

C. Pressure Distribution on a Family of Slotted Disks

In view of the interesting nature of the drag curves given in Fig. 8, and the apparent drag increase for small amounts of porosity (see test C6A in Fig. 8), it was decided to mount a thorough investigation of the pressure distribution on the family of porous, slotted disks.

Table 1 Geometric definition of the Sandia porous disks

Configuration no.	No. of radial slots	Outside diam of disk, in.	Radius to inside inner slot, in.	Average slot width, in.	Average solid width between slots, in.	Distance from outside of outer slot to disk edge, in.	Average circumferential distance between slots, in.	Geometric porosity, %
1	0	8.998	–	–	–	–	–	0
2	6	9.002	0.615	0.109	0.559	0.437	0.208	13.72
3	6	9.018	0.588	0.156	0.513	0.418	0.258	19.04
4	6	9.002	0.560	0.221	0.448	0.204	0.204	27.44
5	6	9.036	0.529	0.277	0.392	0.368	0.265	33.04
5A	1	9.036	2.539	0.277	–	1.702	0.267	6.42
6	18	9.006	0.396	0.093	0.130	0.220	0.256	34.33
6A	1	9.006	2.640	0.093	–	1.770	0.260	2.22

Notes: 1) Configurations 5 and 6 have same nominal porosity with the mean location of three slots in configuration 6 located exactly on one slot of configuration 5. Configuration 5A uses only the 4th slot of configuration 5. Configuration 6A uses only the 11th slot of configuration 6. All geometric measurements at 65° F.

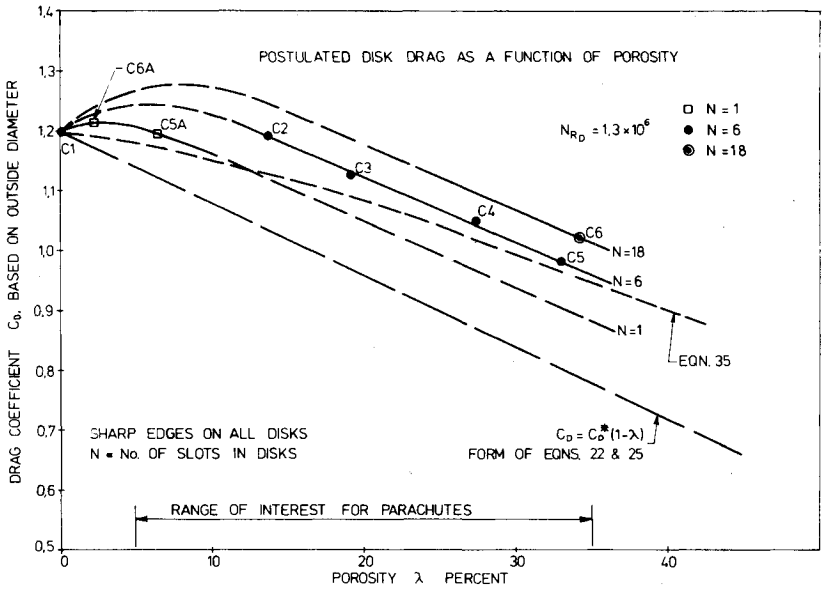

Fig. 8 Drag coefficients.

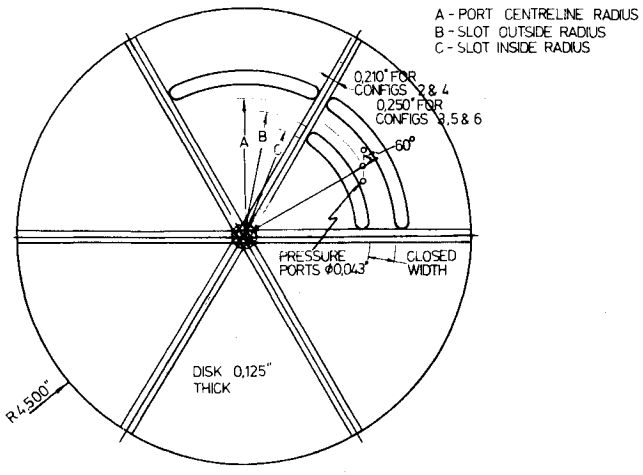

Fig. 9 Disk details.

The definition of the disk configurations is given in Fig. 9 which should be read in conjunction with Table 1. In general, a set of 9-in. diam 45 deg chamfered disks were slotted with one, six, or eighteen sets of coaxial slots. Holes were introduced between each slot to form pressure ports. Care was taken to correctly locate the holes and to remove all burrs from the ports. The location of the pressure ports can be ascertained from the appropriated plots of the pressure distributions.

The disks were sting mounted in the 7×10 ft low-speed wind tunnel facility at the Vought Corporation in Dallas. The disks were mounted on a tapered sting, which terminated in a 1 in. fitting. It was suitably stayed and small blockage corrections were applied to all the test data.

A solid disk was tested initially and the drag coefficient confirmed with the standard drag coefficient given by Hoerner.[4]

Next, the solid disk, configuration 1, was pressure plotted at a Reynolds number of 1.3×10^6. All subsequent tests reported herein have been conducted at this same Reynolds number. The pressure distribution on the solid disk is shown in Fig. 10. It should be noted that the base pressure is -0.45 and substantially uniform.

The next test involved configuration 6A. Here, the overall porosity is 2.22% and the number of slots N is unity. This slot was located at a radius ratio ξ of about 0.6. The pressure distribution is shown in Fig. 11; it will be noticed that the base pressure coefficients on each side of the slot are -0.45 and about -0.55. The slot location is shown on the abscissa. It is important in what is to follow to appreciate that there is a pressure discontinuity across the slot. In this case the jump in C_p across the slot is about 0.1. Finally, the solid disk pressure distribution is shown by the dotted curve in Fig. 11. It can be seen that the small slot has substantially modified the base pressure coefficients.

The next logical configuration was 5A. Again there was only one slot ($N=1$), but, as previously, the porosity had been increased to 6.42% at the same slot location. In this case two stable pressure configurations were measured. The first is

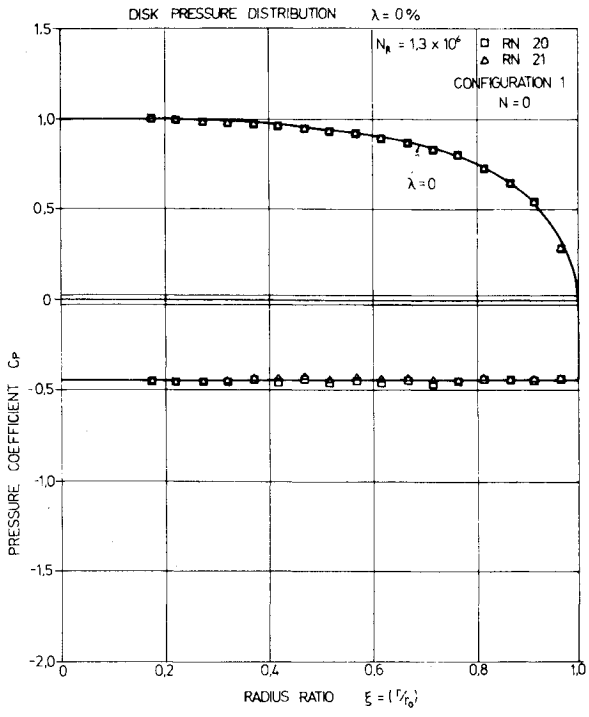

Fig. 10 Pressure distributions.

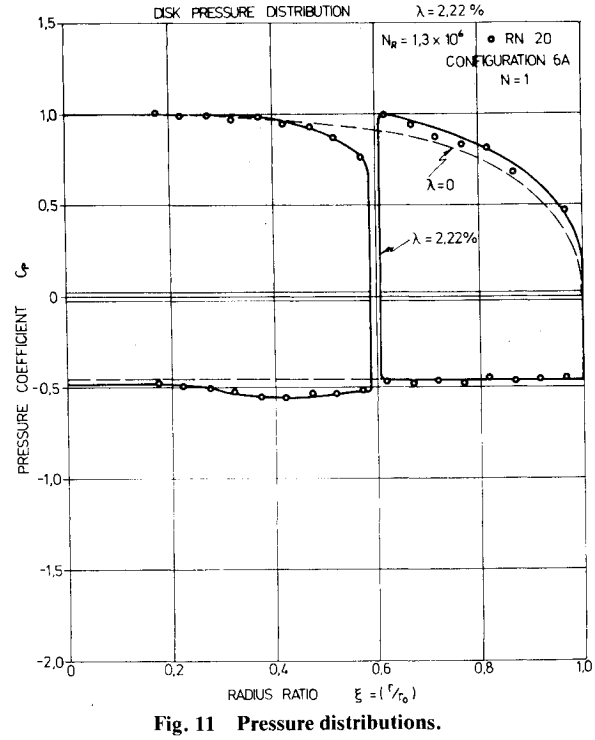

Fig. 11 Pressure distributions.

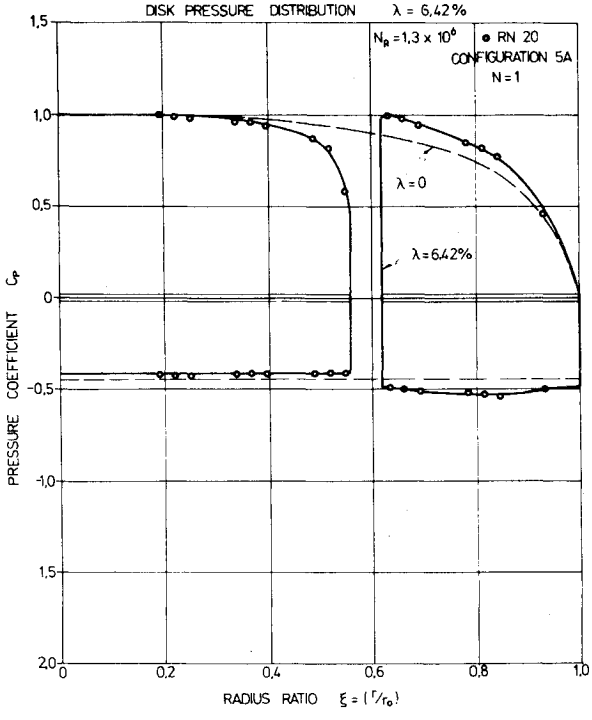

Fig. 12 Pressure distributions.

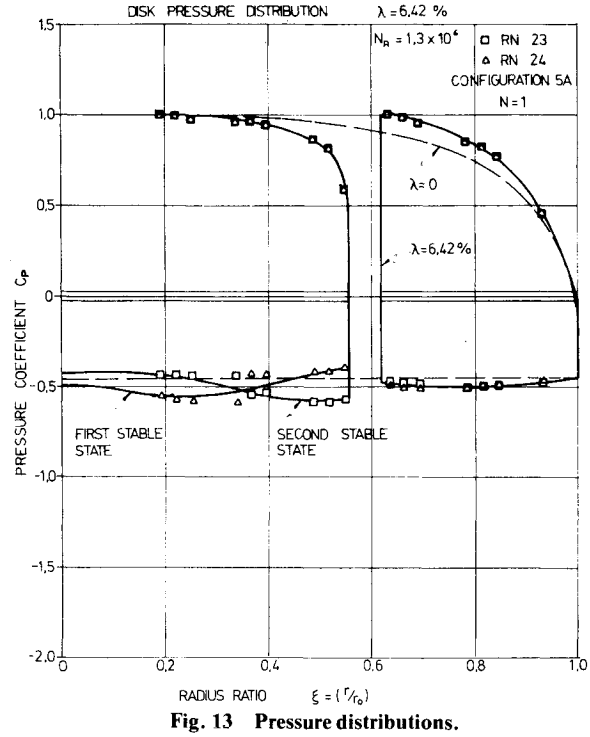

Fig. 13 Pressure distributions.

shown in Fig. 12, where the pressure coefficient discontinuity across the slot is still about 0.1, but the pattern is reversed from that shown in Fig. 11. The second stable configuration is shown by the lower curve in Fig. 13. In fact, Fig. 13 has been used to demonstrate that the two bistable pressure configurations seem to appear randomly when the tunnel is turned off and on again. Thus, we have clearly demonstrated that the discontinuity in pressure across the slot is a real effect, and can exist with a rising or falling jump in the magnitude of the pressure across the single slot.

We now move on to an examination of a disk with six slots, where each slot is of constant width, as shown along the abscissa of Fig. 14. The overall porosity was 33.04% and the configuration number was 5. In this test the discontinuity still persisted across each slot. Also, it was about the same magnitude, but the bistable nature of the arrangement no longer appeared to exist. It should be noted that the mean base pressure coefficient has reduced dramatically to about -0.7, compared to the solid disk value of only -0.45. Therefore, it is not surprising that the drag increases in Fig. 8 which can be attributed to this falling base pressure coefficient.

Finally, to put the issue beyond doubt, a further experiment was devised. This experiment maintained the porosity con-

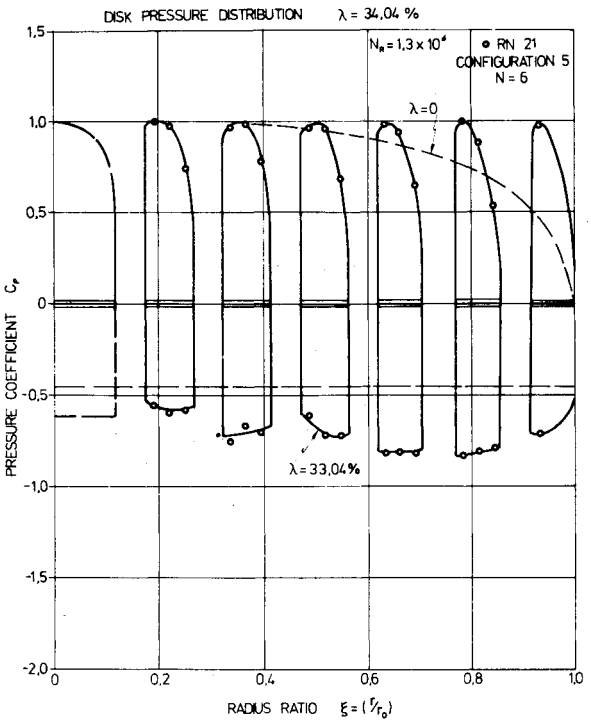

Fig. 14 Pressure distributions.

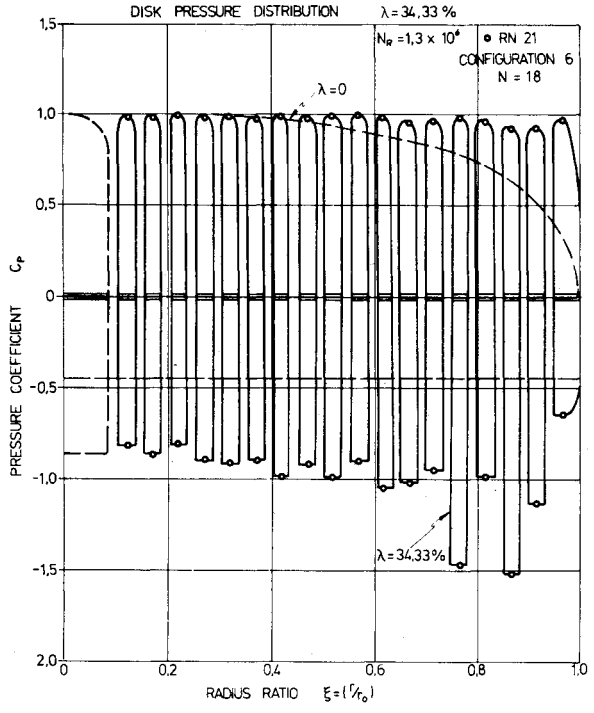

Fig. 15 Pressure distributions.

stant (namely, 34.33%), but increased the number of annular slots from 6 to 18. The arrangement is listed as configuration 6. In this case, the pressure distribution is shown in Fig. 15. It can be seen therein that the base pressure coefficient has fallen to a minimum value of about -1.5 near the outer edge, while the mean base pressure coefficient stands at about -1.0 compared to -0.45 for a solid disk. Therefore, there is no doubt that the drag coefficient is not uniquely determined by the porosity alone, but also by the precise details of the slot arrangement. Furthermore, this is not a Reynolds number effect, but it is believed to be a coanda-type effect resulting from the jets issuing from between the slots. This latter point will now be discussed.

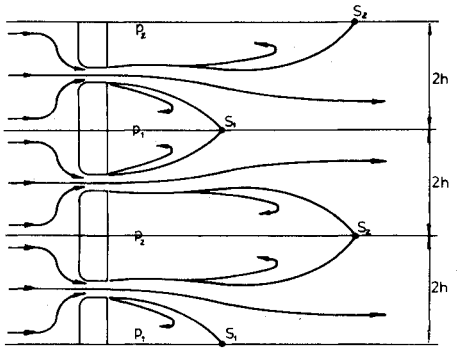

Fig. 16 An actual flow through a porous screen.

D. Jet Entrainment or Coanda Effects in Porous Body Flow

The effects of entrainment in confined jet flow has been extensively studied by Sawyer.[22] It is asserted here that the jet phenomenon is dominant in the wake flow behind these disks. As these jets issue behind the disk (or, in fact, from a two-dimensional screen), the turbulent entrainment effects cause the jets to coalesce and thereby produce strong, local negative pressure regions.

Sawyer[22] has considered jets issuing parallel and adjacent to a flat plate. Here the jet attaches to the plate downstream of the jet origin. Roberts[13] has considered a similar flow where a two-dimensional jet issues into a parallel channel.

If in two-dimensional flow one were to consider an infinite number of reflections of the flow in the channel walls, then one can produce an infinite or finite porous screen flow. This system is shown in Fig. 16.

In Fig. 16, fluid issues from between elements to form a series of jets. The idealized, bistable arrangement is for adjacent jets to coalesce forming stagnation points at S_1 and S_2, with local low-pressure separation bubbles of pressure p_1 and p_2. The jet entrainment or coanda effects maintain the pressure discontinuity across each jet. While this effect is not new, no evidence could be found of it being observed in connection with slotted disks or parachutes.

It is not proposed to examine the jet flows in the present paper. The phenomenon is reported only as experimental evidence. Further extension of the Sawyer[22] type analysis to axisymmetric flows will be left to a subsequent publication.

III. Conclusion

One can conclude by asserting that it is believed that the coanda or jet entrainment effects are dominant in the flow through and immediately behind low-porosity aerodynamic bodies, such as these disks or parachutes. In the parachute context this phenomenon has not been raised before. Further research should be directed in this direction.

Some of the most intriguing experimental results have been reported in Figs. 8-15 and an independent confirmation of these tests would be appreciated.

Acknowledgments

The author wishes to express his appreciation to Sandia Laboratories, Albuquerque, N. Mex., for their provision of sabbatical leave facilities. In particular, he wishes to thank R. Tate and R. Palmer of the Aerodynamics Division for their assistance in collecting and reducing the wind tunnel data at LTV.

References

[1] Taylor, G.I. and Davies, R.M., "The Aerodynamics of Porous Sheets," *Scientific Papers of G.I. Taylor,* Vol. III, pp. 391-405.

[2] Morgan, P.M., "Fluid Flow Through Screens of Low Porosity," *Journal of the Royal Aeronautical Society,* Vol. 66, 1962.

[3] Perry, "Study of the Effects of Fabric Geometry on Air Permeability," WADC Tech. Rept. 54-574, 1955.

[4] Hoerner, S.F., *Fluid Dynamic Drag,* 1965, pp. 3-23.

[5] Brown, W.D., "The Effect of Tension on the Porosity of a Parachute Fabric," Royal Aircraft Establishment, TN 1356.

[6] McVey, D.F., Pepper, W.B., and Reed, J.F., "A Parametric Wind Tunnel Study of Ribbon Parachutes," AIAA Paper 75-1370, Albuquerque, N. Mex., Nov. 17-19, 1975.

[7] Graham, J.M.R., "Turbulent Flow Past a Porous Plate," *Journal of Fluid Mechanics,* Vol. 73, Pt. 3, pp. 565-591, 1976.

[8] Hoerner, S.F., *Fluid Dynamic Drag,* 1965.

[9] Taylor, G.I., "Resistance of a Flat Plate of Very Porous Material," *Scientific Papers of G.I. Taylor,* Cambridge University Press, Vol. III, pp. 383-386.

[10] Cockrell, D.J. and Huntley, I.D., "Aerodynamic and Inertial Forces on Model Parachute Canopies," AIAA Paper 75-1371, Albuquerque, N. Mex., Nov. 17-19, 1975.

[11] Milne-Thompson, L.L., *Theoretical Hydrodynamics Macmillan, London, 1968.*

[12] Roberts, B.W., "The Steady Flow Through a Cascade of Closely Spaced Circular Cylinders," *Journal of the Royal Aeronautical Society,* Sept. 1966, pp. 886-887.

[13] Roberts, B.W., "Low Frequency Aeroelastic Vibrations in a Row of Circular Cylinders," Mechanical Engineering Science Monograph No. 4, Sept. 1966.

[14] Nhan, P.T., "Symmetric Vortex Separation Flow on Open Wedges," Graduation Thesis, Univ. of Sydney, 1975.

[15] Thwaites, B., *Incompressible Aerodynamics,* Oxford Univ. Press, England, 1960.

[16] Koo, J.K. and James, D.F., "Fluid Flow Through and Around a Screen," *Journal of Fluid Mechanics,* Vol. 60, Pt. 3, 1973, pp. 513-538.

[17] Gurevich, M.I., *Theory of Jets in an Ideal Fluid,* Pergamon Press, New York, 1966.

[18] Betz, Von, A. and Petersohn, E., "Anwendung der Theorie der Freien Strahlen," Ing. Arch. Vol. 2, 1931, pp. 190-211.

[19] Brikhoff, G., Plesset, M., and Simmons, N., "Wall Effects in Cavity Flows—I and II," *Quarterly of Applied Mathematics,* Vol. 8, No. 2, 1950, pp. 151-168. *Quarterly of Applied Mathematics,* Vol. 11, No. 4, 1952, pp. 413-421.

[20] Sedov, L.I., *Two Dimensional Problems in Hydrodynamics and Aerodynamics,* Interscience Publishers, New York, 1965.

[21] Ambrovii, "Flow about n Parallel Flat Plates," Papers of II Mathematical Congress, 1931, pp. 304-310.

[22] Sawyer, R.A., "The Flow of a Two-Dimensional Jet Issuing Parallel to a Flat Plate," *Journal of Fluid Mechanics,* Vol. 9, 1960, pp. 543-560.